

# Velocity and Surface Shear Stress Distributions Behind a Rough-to-Smooth Surface Transition: A Simple New Model

Leonardo P. Chamorro · Fernando Porté-Agel

Received: 11 July 2008 / Accepted: 10 November 2008  
© Springer Science+Business Media B.V. 2008

**Abstract** A simple new model is proposed to predict the distribution of wind velocity and surface shear stress downwind of a rough-to-smooth surface transition. The wind velocity is estimated as a weighted average between two limiting logarithmic profiles: the first log law, which is recovered above the internal boundary-layer height, corresponds to the upwind velocity profile; the second log law is adjusted to the downwind aerodynamic roughness and local surface shear stress, and it is recovered near the surface, in the equilibrium sublayer. The proposed non-linear form of the weighting factor is equal to  $\ln(z/z_{01})/\ln(\delta_i/z_{01})$ , where  $z$ ,  $\delta_i$  and  $z_{01}$  are the elevation of the prediction location, the internal boundary-layer height at that downwind distance, and the upwind surface roughness, respectively. Unlike other simple analytical models, the new model does not rely on the assumption of a constant or linear distribution for the turbulent shear stress within the internal boundary layer. The performance of the new model is tested with wind-tunnel measurements and also with the field data of Bradley. Compared with other existing analytical models, the proposed model shows improved predictions of both surface shear stress and velocity distributions at different positions downwind of the transition.

**Keywords** Atmospheric boundary layer · Large-eddy simulation · Roughness transition · Surface shear stress model

## 1 Introduction

Understanding the effects of surface roughness transitions on the spatial distribution of surface shear stress and velocity is key to improving predictions of turbulent transport in the

---

L. P. Chamorro · F. Porté-Agel (✉)  
Saint Anthony Falls Laboratory, Department of Civil Engineering, University of Minnesota,  
2, Third Avenue SE, Minneapolis, MN 55414, USA  
e-mail: fporte@umn.edu

F. Porté-Agel  
National Center for Earth-Surface Dynamics, Minneapolis, MN, USA

atmospheric boundary layer (ABL). For example, most atmospheric numerical models require as a lower boundary condition the specification of the surface shear stress as a function of the grid-averaged velocity field. In large-scale numerical models, such as weather and climate models, the surface boundary condition needs to account for the effects of subgrid surface heterogeneity on the spatial distribution of the surface shear stress and its relation with the velocity in the surface layer (Wieringa 1986; Taylor 1987; Mason 1988; Claussen 1990; Bou-Zeid et al. 2004). In the case of higher resolution numerical models, such as large-eddy simulation (LES), where much of the surface heterogeneity is explicitly resolved, the surface boundary condition still requires the calculation of the local (spatially filtered) surface shear stress as a function of the filtered fluctuating velocity at the lowest computational grid points. Currently, these models rely on the application of Monin-Obukhov similarity theory (the logarithmic law under neutral conditions) using local values of the filtered velocity. However, the accuracy of this approach is questionable since similarity theory is strictly valid only when applied over homogeneous surfaces and considering averaged quantities. Improvement of these boundary condition parameterizations in simulations of ABL flow over heterogeneous surfaces requires a better understanding of the effects of surface roughness transitions on the relation between surface shear stress and velocity fields.

Several models with different levels of complexity have been proposed to estimate the spatial distribution of surface shear stress and velocity after a roughness transition (e.g. Elliott 1958; Mulhearn 1978; Panofsky and Townsend 1964; Townsend 1965, 1966). The simplest and most common analytical models, introduced by Elliott (1958) and Panofsky and Townsend (1964), were obtained assuming a constant and a linear vertical distribution (respectively) of the friction velocity within the internal boundary layer (IBL). Rao et al. (1973) used a numerical approach based on the Reynolds-averaged Navier-Stokes equations with a second-order closure model that includes a set of differential transport equations for the components of the Reynolds stress tensor. Rao's simulated velocity and surface shear stress profiles showed good agreement with the experimental field measurements of Bradley (1968). Recently, Bou-Zeid et al. (2005) used a small computational domain to perform a very high resolution large-eddy simulation of the same roughness transitions using Lagrangian dynamic subgrid-scale models and showed that the simulated surface shear stress fields agreed reasonably well with the experimental field data of Bradley (1968).

A common simple approach used to relate surface shear stress and velocity in the surface layer is Elliott's model (Elliott 1958), which assumes that the downwind velocity profile is in equilibrium with the new surface and, therefore, follows a logarithmic profile all the way up to the top of the internal boundary layer (height  $\delta_i$ ),

$$U = \frac{u_{*2}}{k} \ln \left( \frac{z}{z_{02}} \right), \quad (1)$$

where  $U$  is the average velocity at elevation  $z$ ,  $u_{*2}$  is the friction velocity,  $z_{02}$  is the downwind surface roughness, and  $k$  is the von Kármán constant. This equation can be derived by assuming a constant shear stress along the vertical for  $z < \delta_i$  and an equilibrium value of unity for the nondimensional wind shear  $\Phi_m = (kz/u_{*2})(\partial U/\partial z)$ . For time-averaged surface shear stress ( $\tau_s$ ) predictions, Eq. (1) can be written as

$$\tau_{s2} = - \left[ \frac{kU}{\ln(z/z_{02})} \right]^2, \quad (2)$$

where  $u_{*2} = \sqrt{-\tau_{s2}}$ . It is important to note that, due to a constant vertical turbulent shear stress assumption, this model produces an unrealistically sharp stress discontinuity at the top

of the internal boundary layer  $z = \delta_i$ . For the IBL depth  $\delta_i$ , Elliott proposed the following relation:

$$\eta = (0.75 - 0.03M') \xi^{0.8}, \tag{3}$$

where  $\eta$ ,  $M'$  and  $\xi$  are non-dimensional parameters defined as  $\eta = \delta_i/z_{02}$ ,  $M' = \ln(z_{02}/z_{01})$  and  $\xi = x/z_{02}$ ,  $z_{01}$  and  $z_{02}$  are the upwind and downwind aerodynamic surface roughness, respectively, and  $x$  is the distance measured from the roughness change.

To avoid an abrupt change in the surface shear stress at the internal boundary-layer height  $\delta_i$ , Panofsky and Townsend (1964) considered a linear variation of the friction velocity with respect to height within the IBL:

$$u_* = u_{*1} \left[ (1 - S) + S \frac{z}{\delta_i} \right], \tag{4}$$

where  $S = (u_{*1} - u_{*2})/u_{*1}$  is a nondimensional measure of the relative change in surface stress associated with the transition, and  $u_{*1}$  and  $u_{*2}$  are the upwind and downwind friction velocity respectively.

As in Elliott’s model, the velocity and surface shear stress distributions are derived by assuming a value of unity for the nondimensional wind shear. This yields

$$\begin{aligned} U &= \frac{u_{*1}}{k} \left[ (1 - S) \ln \left( \frac{z}{z_{02}} \right) + S \frac{z}{\delta_i} \right] \Leftrightarrow \\ U &= \frac{u_{*2}}{k} \ln \left( \frac{z}{z_{02}} \right) + \frac{u_{*1} - u_{*2}}{k} \left( \frac{z}{\delta_i} \right), \end{aligned} \tag{5}$$

which implies

$$\frac{\tau_{s2}}{\tau_{s1}} = \left[ 1 - \frac{kU/u_{*1} - \ln(z/z_{02})}{z/\delta_i - \ln(z/z_{02})} \right]^2, \tag{6}$$

where  $\tau_{s1}$  and  $\tau_{s2}$  are the upwind and downwind surface shear stresses, respectively. Note that Panofsky and Townsend’s model (hereon referred also as P-T) requires an explicit estimation for the internal boundary-layer height  $\delta_i$ . Panofsky and Townsend (1964) proposed an IBL depth-fetch relationship given by

$$\begin{aligned} 4k^2(\xi - \xi_0)/\eta &= \ln\eta - 5 + \frac{1}{2}M + \frac{4 - \frac{7}{6}M - \frac{1}{4}M^2}{\ln\eta - 1 + \frac{1}{4}M} \\ &+ \frac{4 + \frac{7}{6}M + \frac{1}{24}M^2 + \frac{1}{16}M^3}{(\ln\eta - 1 + \frac{1}{4}M)^2}, \end{aligned} \tag{7}$$

where  $M = \ln(z_{01}/z_{02})$  and  $\xi_0 = 0$  for  $M = 1.65$  (smooth-to-rough transition) and  $M = 2.17$  (rough-to-smooth transition). A recent review on this and other IBL height models can be found in Savelyev and Taylor (2005).

Experience suggests that the predictions from both Elliott and P-T models can differ substantially from observations. This can be explained considering that, as shown by Rao et al. (1973), the non-dimensional wind shear, dissipation length scale, mixing length scale, and ratio of stress to turbulent kinetic energy downwind of a roughness transition are found to differ significantly from their equilibrium values.

In this paper, a simple new analytical model is proposed to predict the spatial distribution of wind velocity and surface shear stress downwind of a rough-to-smooth surface transition. First, a wind-tunnel experiment is presented in Sect. 2. The experiment was designed to study

the performance of different simple analytical models. In Sect. 3, the models of Elliott and Panofsky–Townsend are tested, the proposed alternative new simple model is presented in Sect. 4, and its performance is evaluated in Sect. 5 using our wind-tunnel data as well as Bradley’s field data. Finally, a summary is given in Sect. 6.

## 2 Experimental Set-up

A rough-to-smooth surface transition has been designed and installed in the boundary-layer wind tunnel of the Saint Anthony Falls Laboratory at the University of Minnesota, U.S.A. with the goal of studying the performance of different models for the spatial distribution of wind velocity and surface shear stress downwind of the transition. The boundary-layer wind tunnel has a plan length of 37.5 m with a main test section fetch of roughly 15 m. There is a contraction with a 6.6:1 area ratio upwind of the test section along with flow conditioning/turbulence control consisting of a coarse wire mesh and honeycomb flow-straightened. The tunnel is driven by a 200 horse-power fan and is operated as a closed return loop. The turbulence intensity in the centre of the wind tunnel is approximately 0.25% for a  $10 \text{ ms}^{-1}$  freestream flow speed. More details on the wind tunnel can be found in [Carper and Porté-Agel \(2008\)](#).

Wind-tunnel flow velocity was measured using Pitot static tubes (mainly for calibration) and constant temperature anemometry (CTA). Two types of CTA were considered: single-normal (SN) and crosswire (XW or x-wires) probes. The probes are made with  $5.0 \mu\text{m}$  tungsten wire and are connected to an A.A. Lab Systems AN-1003 10-channel CTA system. During the calibration and measurements the temperature fluctuations were kept within a  $\pm 0.5^\circ\text{C}$  range to avoid bias errors due to thermal drift of the voltage signal.

The rough-to-smooth transition was created by placing 7 m length of wire mesh on the wind-tunnel floor upstream of a smooth flat plate. The woven-wire mesh is considered a k-type roughness (see [Jimenez 2004](#)) and has an average height  $k_0 = 3 \text{ mm}$  with an aerodynamic roughness length  $z_{01} = 0.5 \text{ mm}$ .

A turbulent boundary layer is developed upstream with the help of a tripping mechanism (80 mm picket fence) located at the exit of the wind-tunnel contraction where the test section begins. The turbulent boundary layer is allowed to grow in zero pressure gradient conditions by adjustment of the wind-tunnel ceiling. The upstream roughness induces a strong change in the momentum flux near the surface, maintaining a well-developed surface layer with constant shear stress and a logarithmic velocity profile. The experiments were conducted with a  $10 \text{ ms}^{-1}$  freestream flow velocity and a turbulent boundary-layer depth of  $\delta = 0.4 \text{ m}$  at the roughness transition location.

A SN hotwire (boundary-layer type) probe and a crosswire anemometer were used to measure surface shear stress and wind velocity (respectively) at different positions downstream of the transition ( $x/\delta = 0.1, 0.15, 0.2, 0.25, 0.375, 0.5, 0.75, 1.0$  and  $1.5$ ) and various heights (for the crosswire) within the internal boundary layer. A schematic and photograph of the experimental set-up are shown in [Fig. 1](#). The single hotwire was placed in the viscous sub-layer, directly over the smooth surface. This procedure is well established and has been used in previous experimental studies by [Alfredsson et al. \(1988\)](#); [Chew et al. \(1998\)](#) and [Khoo et al. \(1998\)](#). Here, the sensor was calibrated against a Preston tube following the procedure introduced by [Patel \(1965\)](#). During data collection the two sensors’ voltage signatures were sampled simultaneously at a rate of 20 kHz for a measurement period of 60 s.

A review of rough-wall boundary layers by [Jimenez \(2004\)](#) and an experimental study by [Castro et al. \(2006\)](#) suggest that the boundary layer behaves differently depending on the

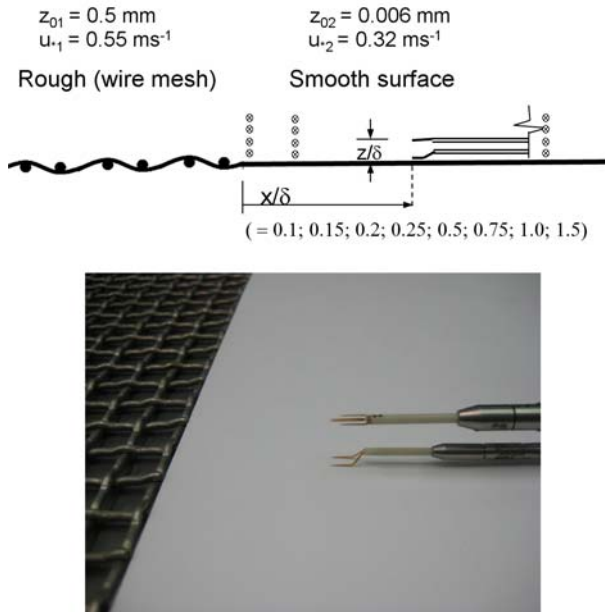


**Fig. 1** Schematic of the rough-to-smooth transition and measurement locations (*top*) and photograph of the single hotwire and crosswire probes placed downwind of the surface transition (*bottom*)

ratio of boundary-layer height ( $\delta/k_0$ ), with a change in behaviour when  $\delta/k_0 > 80$ , which is typical for the ABL. Previous wind-tunnel experiments (Antonia and Luxton 1972; Mulhearn 1978; Cheng and Castro 2002; Castro et al. 2006) have provided valuable results but use  $\delta/k_0$  on the order of 20. These relatively low ratios of boundary-layer height to roughness element height are not typical for land surface transitions because the effect of their roughness elements reaches further into the wind-tunnel boundary layer than does the effect of rough terrain in the ABL. Thus, the roughness chosen in those wind-tunnel studies may not provide a large enough range of length scales to allow a true equilibrium surface layer to develop. The set-up used in this study maintains a  $\delta/k_0 = 133$  to ensure that inner and outer scales of the boundary layer, and hence its structure, are well developed.

The zero pressure gradient boundary layer, developed upstream of the transition, had a Reynolds number based on the surface shear stress of  $Re_\nu = u_*\delta/\nu \approx 1.5 \times 10^4$ , a boundary-layer thickness of  $\delta = 0.4$  m, a friction velocity of  $u_{*1} = 0.55$  m s $^{-1}$  and a freestream velocity  $U_1 = 10$  m s $^{-1}$ . In this condition, the upwind transition boundary layer is in the fully rough regime (Jimenez 2004). The smooth surface consists of the finished wooden floor of the tunnel with a window of flat plate that lies flush and sealed with the floor. A boundary layer forming over only the smooth floor has approximately the same height as the boundary layer over the rough surface but with a friction velocity  $u_{*2} = 0.32$  m s $^{-1}$ .

Calibrations of the single and crosswire anemometers were performed at the beginning of the experiment run. The crosswire was calibrated in the freestream region against a Pitot-static probe, at seven angles for each of seven velocities. A cubic-spline table calibration method was then used to determine the two instantaneous velocity components from the two instantaneous voltage signatures. For more details on the crosswire calibration see Bruun (1995). Calibration of the single hotwire against a Preston tube (Patel 1965) was carried out

using ten different velocities. The single hotwire and Preston tube were placed over a smooth flat plate in the freestream region to avoid any disturbance.

### 3 Analysis of Elliott and Panofsky–Townsend Models for Surface Shear Stress

The average surface shear stress measured with the single hotwire, normalized with the equilibrium downwind surface shear stress ( $\tau_o$ ), is plotted in Fig. 2 as a function of the normalized distance downwind from the transition. As expected, the shear stress increases with distance from the transition and asymptotes to the equilibrium shear stress on the smooth surface. At a distance slightly larger than the boundary-layer depth, the shear stress is close to its equilibrium value. The surface shear stress predicted with the Elliott and P–T models, using the velocity measured at a height of  $z = 13.5$  mm in Eqs. 2 and 6, respectively, are also plotted in Fig. 2 for comparison. Both models clearly underestimate the value of the surface shear stress at each of the downwind locations under consideration.

It is important to notice that P–T’s surface shear prediction should always be smaller than Elliott’s prediction when they are based on the velocity at the same height. This is due to the fact that the P–T model (Eq. 5) adds a positive term to Elliott’s velocity relation, which necessarily implies a lower surface shear stress.

Ideally, the surface shear stress prediction, obtained with any given model, should have no (or small) dependence on the height at which the velocity is measured. Figure 3 shows Elliott’s surface shear stress prediction at different downwind positions using velocities measured at different heights. From this it is clear that Elliott’s surface shear stress prediction is strongly dependent on the height at which the model is applied. It is interesting to note that the prediction improves as the considered height approaches the IBL height. P–T’s surface shear stress predictions were also found to have a similar strong dependence (not shown here) on the height at which the model is applied.

A particular case of Elliott’s approach is given by Jensen (1978), who proposed an expression for the ratio between downwind and upwind shear stresses ( $\tau_{s2}/\tau_{s1}$ ) based on applying Elliott’s equation at  $z = \delta_i$ :

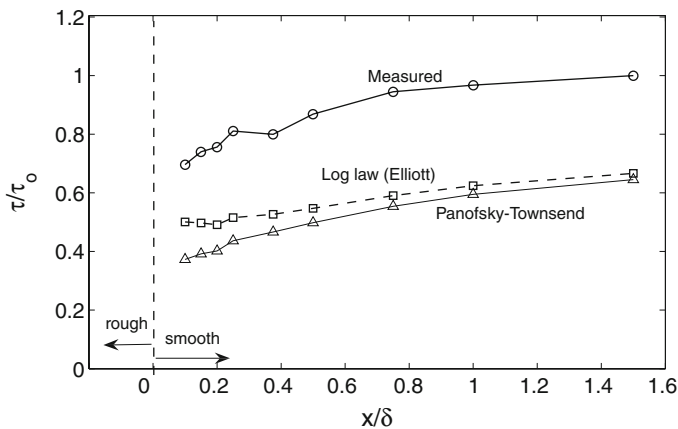


**Fig. 2** Comparison between measured average surface shear stress and the predictions from the models of Elliott (Eq. 2) and Panofsky–Townsend (Eq. 6). Downwind distance is normalized with the boundary-layer height  $\delta = 0.4$  m. Surface shear stress is normalized with its downwind equilibrium value ( $\tau_o$ )

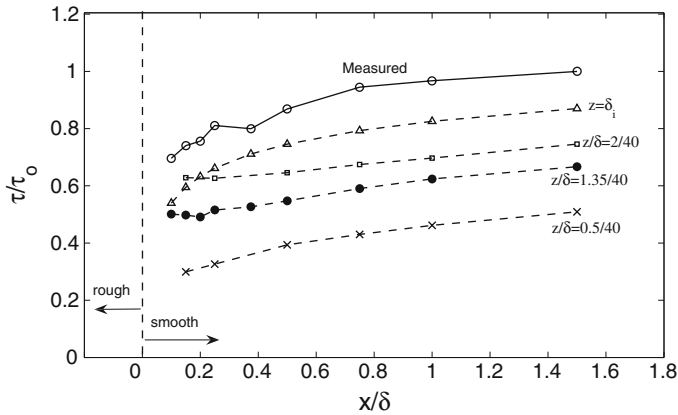


**Fig. 3** Measured and modelled surface shear stress obtained with Elliott’s log-law model (Eq. 2) using velocity measurements at different heights  $z$ . Downwind distance and height are normalized using the boundary-layer height  $\delta = 0.4$  m. Surface shear stress is normalized with its downwind equilibrium value ( $\tau_0$ )

$$\frac{\tau_{s2}}{\tau_{s1}} = \left[ 1 - \frac{M}{\ln(\delta_i/z_{02})} \right]^2 \tag{8}$$

As shown in Fig. 3, this relation yields the right trend in the surface shear stress, but (in this case) it underestimates its magnitude by about 15% at all positions downwind of the transitions. It is important to note that, in order to use this model, an estimate for the internal boundary-layer height is required. In Fig. 3, for the case of  $z = \delta_i$  (Jensen’s model), the IBL growth equation proposed by Elliott (Eq. 3) has been used. Note that, unlike Elliott and P–T parameterizations, Jensen’s model cannot predict the velocity distribution throughout the IBL.

Previous studies (e.g. Bradley 1968) suggest that vertical velocity profiles downwind of a roughness transition have a log-nonlinear behaviour, which differs from the log-linear models of Elliot and P–T. Next we propose a simple model that attempts to reproduce the log-nonlinear velocity distribution pattern observed within the internal boundary layer.

#### 4 Alternative Simple Model for Velocity and Surface Shear Stress Predictions

As pointed out by Garratt (1990), the observed behaviour of velocity profiles within internal boundary layers suggests that they might be described through a modified logarithmic law of the general form

$$U = \frac{u_{*2}}{k} \ln\left(\frac{z}{z_{02}}\right) + f(z/\delta_i), \tag{9}$$

where the function  $f(z/\delta_i)$  should have the following limiting values

$$f = \begin{cases} \left(\frac{u_{*1}}{k}\right) \ln\left(\frac{z}{z_{01}}\right) - \left(\frac{u_{*2}}{k}\right) \ln\left(\frac{z}{z_{02}}\right), & z/\delta_i \geq 1 \\ 0, & z/\delta_i \ll 1. \end{cases} \tag{10}$$

The limiting values for  $f(z/\delta_i)$  reflect the effect of boundary conditions given by the upstream logarithmic velocity profile at  $z/\delta_i$  and the equilibrium logarithmic velocity profile close to the downwind surface.

One possible simple formulation for the function  $f(z/\delta_i)$  that satisfies the conditions given by Eq. 10 can be obtained by weighting the function  $f(z/\delta_i)$  by a nondimensional parameter  $\lambda$  such that  $0 < \lambda < 1$  for  $z/\delta_i < 1$ . This yields the following equation for the velocity distribution within the IBL:

$$U \approx \frac{u_{*2}}{k} \ln\left(\frac{z}{z_{02}}\right) + \lambda \left( \frac{u_{*1}}{k} \ln\left(\frac{z}{z_{01}}\right) - \frac{u_{*2}}{k} \ln\left(\frac{z}{z_{02}}\right) \right), \tag{11}$$

which can also be written as

$$U \approx (1 - \lambda) \frac{u_{*2}}{k} \ln\left(\frac{z}{z_{02}}\right) + \lambda \frac{u_{*1}}{k} \ln\left(\frac{z}{z_{01}}\right). \tag{12}$$

Note that Eq. 12 implies that  $u(z)$  is estimated as a combination of two limiting log laws, one corresponding to the upwind velocity profile and the second corresponding to the so-called equilibrium sublayer, where the flow is in equilibrium with the downwind surface. In order to satisfy the conditions given in Eq. 10, the weighting parameter  $\lambda$  should increase monotonically as  $z/\delta_i$  increases. Our wind-tunnel measurements (Fig. 4) and also previous studies (e.g., Bradley 1968) suggest that  $\lambda$  does not follow strictly a linear relation in terms of  $z/\delta_i$ . In order to obtain a simple expression for the non-dimensional parameter  $\lambda$ , it is important to identify the variables that have a dominant effect in the shape of the velocity profile. In addition to  $z$  and  $\delta_i$ , previous studies (e.g. Wood 1982) have shown that the largest of the two aerodynamic roughnesses,  $z_{01}$ , is the more relevant parameter of the two. Taking this into consideration, a simple non-linear monotonically increasing function that satisfies the limiting conditions in Eq. 10 and induces a non-linear log velocity profile behaviour is

$$\lambda = \ln(z/z_{01}) / \ln(\delta_i/z_{01}). \tag{13}$$

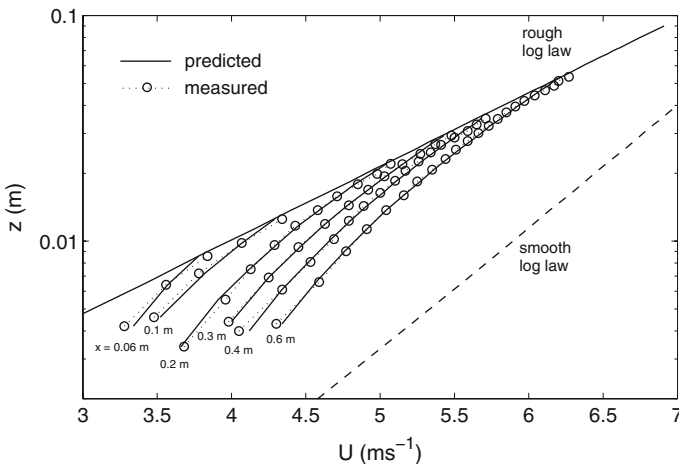


**Fig. 4** Adjustment of wind velocity profiles behind rough-to-smooth transition ( $z_{01} = 0.5$  mm,  $z_{02} = 0.0064$  mm) measured in the wind tunnel (continuous lines correspond to predictions from the new model)

### 5 Evaluation of the New Model

Figure 4 shows a comparison between mean velocity profiles measured downwind of the rough-to-smooth transition and the corresponding profiles estimated using the simple new formulation given by Eqs. 12 and 13. Our results show an excellent agreement between modelled and measured velocities. It is important to observe that the velocity profiles do not follow a logarithmic law within the IBL. In fact, velocity profiles show a clear curvature (log-nonlinear behaviour) that cannot be reproduced by Elliott’s log-law model.

Next, we evaluate the performance of the model to predict the local value of the surface shear stress as a function of the velocity at different locations in the IBL. Figure 5 shows a comparison between the surface shear stress measured at different positions downwind of the surface transition and the estimated surface shear stress obtained using the new formulation with the velocity measured at  $z = 5$  and  $13.5$  mm. For comparison, results from the Elliott’s model are also included. The new model markedly improves the surface shear stress prediction. Moreover, the prediction of the new model shows very small dependence on the height in the IBL at which the model is applied. Despite the remarkable performance of the model to capture the evolution of the surface shear stress near the transition, the model is found to overestimate the value of the equilibrium value of the surface shear stress away from the transition by nearly 15%.

In order to gain further insight on the performance of the new model, in Fig. 6 the value of the parameter  $\lambda$  obtained with the new model (Eq. 12) is compared with the ‘exact’ value calculated from the measured velocity. The value of  $\lambda$  is presented as a function of distance from the transition ( $x/\delta_i$ ) and for three different heights ( $z = \text{constant} = 13.5$  mm,  $z/\delta_i = 0.5$ , and  $z/\delta_i = 0.75$ , respectively). Note that for a given height (e.g.,  $z = 13.5$  mm), the value of  $\lambda$  decreases with downwind distance (Fig. 6a). This is consistent with the fact that, at that height, the wind velocity becomes more adjusted to the downwind surface and, consequently, the model should have a larger relative contribution from the downwind log law (smaller  $\lambda$  in Eq. 12). In Fig. 6b, c the value of  $\lambda$  is nearly constant due to the fact that the height relative

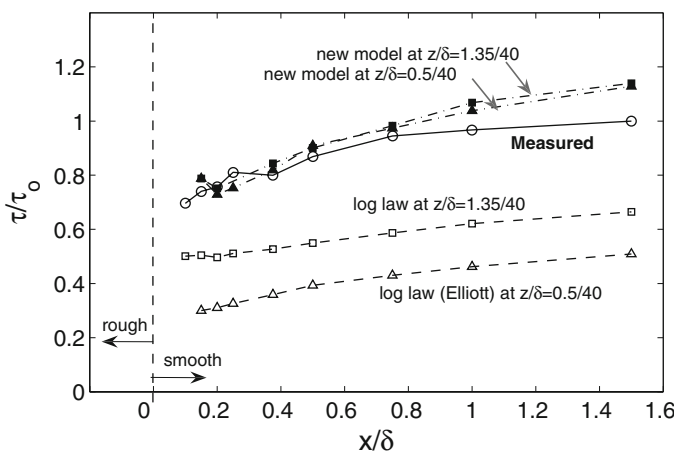


**Fig. 5** Measured and modelled surface shear stress obtained with Elliott’s log-law model (Eq. 2) and the proposed new model using velocity measurements at two different heights. Downwind distance and height are normalized using the boundary-layer height  $\delta = 0.4$  m. Surface shear stress is normalized with its downwind equilibrium value ( $\tau_0$ )

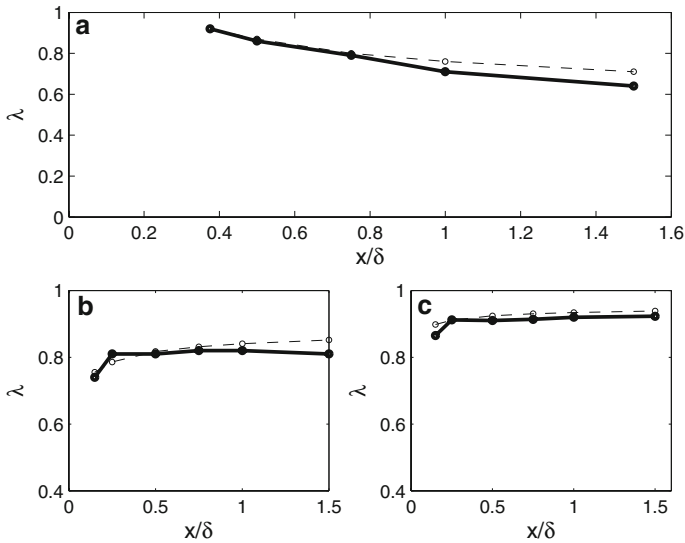


**Fig. 6** Spatial distribution of the weighting factor  $\lambda$  as a function of downwind distance for three different vertical positions: (a)  $z = 13.5$  mm; (b)  $z/\delta_i = 0.5$ ; and (c)  $z/\delta_i = 0.75$ . Dashed lines correspond to the model weighting factor as given by Eq. 13. The solid lines correspond to the 'exact' factor obtained from the measurements

to the boundary layer ( $z/\delta_i$ ) remains constant. In all cases, the new model is able to capture the spatial distribution of  $\lambda$ , which is key to the good performance of the model shown in Figs. 4 and 5.

In order to further test the performance of the new formulation, we have also used the field data of Bradley (1968). In that experimental study, surface shear stress distribution and wind velocity profiles were carefully characterized downwind of a spikes-to-tarmac transition. The surface roughnesses estimated by Bradley (1968) were  $z_{01} = 2.5$  mm for the spikes and  $z_{02} = 0.02$  mm for the tarmac. In a later study, Nemoto (1972) showed that the values of  $z_{01}$ , estimated from Bradley's velocity profiles, range from 1.4 to 0.08 mm and those of  $z_{02}$  range from 0.015 to 0.0023 mm. This was later corroborated by Rao et al. (1973) who reported that values of  $z_{02}$  in the range 0.0002–0.05 mm are equally plausible. He attributed this wide scatter for the smooth surface due to the difficulty associated with extrapolating the neutral equilibrium wind profile data. In this comparison, we follow the same procedure considered by Nemoto (1972), i.e., we analyze each profile and adjust  $z_{01}$  to the velocity profile. The roughness  $z_{02}$  is estimated from the farthest velocity profile, which is better adjusted to the downwind roughness.

Figure 7 shows the comparison between the wind velocity profiles measured by Bradley at different positions ( $x = 2.1, 4.0, 6.1$  and  $8.3$  m) downwind of the transition and the velocity profiles predicted with the new model. The modelled velocity profiles show overall good agreement with the measurements. In Fig. 8, the prediction of the surface shear stress obtained with the new model is compared with the measurements of Bradley for different positions downwind of the surface transition. The modelled shear stress falls within the range of the measurements except for the further distance, where, as in the case of the wind-tunnel comparison, the model appears to slightly overestimate the value of the surface shear stress.

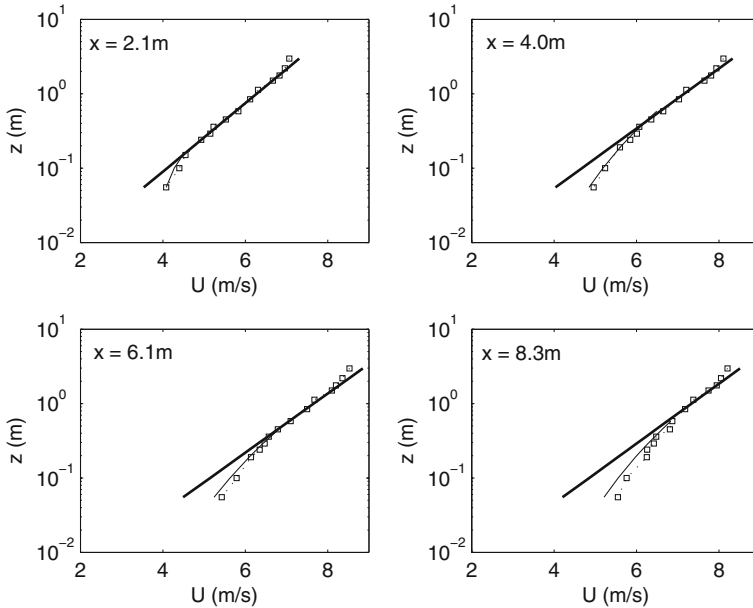


**Fig. 7** Wind velocity profiles behind rough-to-smooth transition. Dotted lines and opens symbols correspond to the measurements of Bradley (1968), while the solid lines are the predictions given by the new model

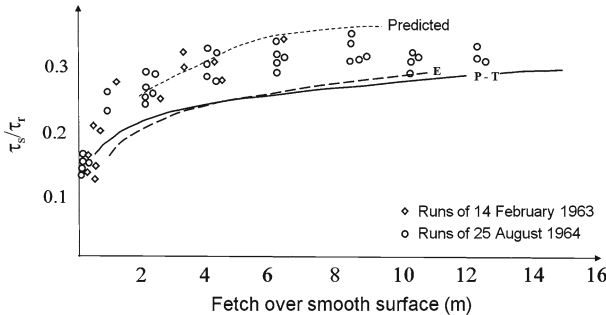


**Fig. 8** Surface shear stress distribution measured in the field experiment of Bradley (1968) (symbols) and corresponding predictions obtained with the new model as well as Elliott’s and P–T’s models. ( $\tau_s$  and  $\tau_r$  are the smooth and rough surface shear stress respectively)

These results contrast with Elliott’s and P–T’s predictions (also presented by Bradley and included in Fig. 8) that systematically underestimate the surface shear stress at all positions.

### 6 Summary

A simple new model is proposed to describe the distribution of wind velocity and surface shear stress downwind of a rough-to-smooth surface transition. The wind velocity is calculated as a weighted average between two limiting logarithmic profiles: the first log law, which is recovered above the internal boundary-layer height, corresponds to the upwind velocity profile; the second log law is adjusted to the downwind aerodynamic roughness and local

surface shear stress, and it is recovered near the surface in the equilibrium sublayer. The proposed non-linear form of the weighting factor is equal to  $\ln(z/z_{01})/\ln(\delta_i/z_{01})$ , where  $z$ ,  $\delta_i$  and  $z_{01}$  are the elevation of the prediction location, the internal boundary-layer height at that downwind distance, and the upwind surface roughness, respectively. Unlike other simple analytical models, the new model does not require the assumption of a constant or linear distribution for the turbulent shear stress within the internal boundary layer. By setting the weighting factor to zero, Elliott's model is recovered.

The performance of the new model is tested with our wind-tunnel measurements and also with the field data of Bradley (1968). The ability of the new model to reproduce both the surface shear stress and the velocity distributions is compared with other existing analytical models, namely Elliott's and P-T's models. These two models are found to underestimate the surface shear stress calculated using the wind velocity measured at different heights within the IBL. In addition, prediction of the surface shear stress obtained with both models shows a strong dependence on height. When the height approaches the internal boundary-layer depth  $\delta_i$ , Elliott's prediction improves. This particular case corresponds to the model of Jensen (1978). However, Elliott's model consistently underestimates the surface shear stress when applied using the velocity at lower locations within the internal boundary layer. This underestimation is even more pronounced for the P-T model due to the fact that, by construction (Eq. 5), P-T's model always predicts a smaller surface shear stress than Elliott's model for any given height and corresponding velocity. The proposed new model yields surface shear stress distributions that are more realistic and, at the same time, have a much smaller dependence on height, compared with the predictions from the models of Elliott and P-T. These results highlight the potential of the new model for use in improved parameterizations for the surface shear stress in large-eddy simulations of turbulent boundary-layer flows over heterogeneous surfaces. The new model is also found to capture the measured downwind evolution of the velocity profiles (including their curvature) with remarkable accuracy.

Future research will focus on developing and testing a similar model for smooth-to-rough surface transitions. In addition, tests will be performed to assess the potential of the new models to be implemented in surface boundary conditions for large-eddy simulations of boundary-layer flow over heterogeneous surfaces. These boundary conditions, used to calculate the local value of the surface shear stress as a function of the velocity, are currently based on direct application of similarity theory (i.e., the log law under neutral stability conditions).

**Acknowledgements** The authors gratefully acknowledge funding from NSF (grant EAR-0537856) and NASA (grant NNG06GE256). Computing resources were provided by the University of Minnesota Supercomputing Institute.

## References

- Alfredsson PH, Johansson AV, Haritonidis JH, Eckelmann H (1988) The fluctuating wall-shear stress and the velocity field in the viscous sublayer. *Phys Fluid* 31:1026–1033
- Antonia RA, Luxton RE (1972) The response of a turbulent boundary layer to a step change in surface roughness. *J Fluid Mech* 53:737–757
- Bou-Zeid E, Meneveau C, Parlange M (2004) Large-eddy simulation of neutral atmospheric boundary layer flow over heterogeneous surfaces: blending height and effective surface roughness. *Water Resources Res* 40:1–18
- Bou-Zeid E, Meneveau C, Parlange M (2005) A scale-dependent Lagrangian dynamic model for large eddy simulation of complex turbulent flows. *Phys Fluid* 17:025105, 18 pp
- Bradley EF (1968) A Micrometeorological study of the velocity profiles and surface drag in the region modified by a change in surface roughness. *Q J Roy Meteorol Soc* 94:361–379
- Bruun HH (1995) *Hotwire anemometry, principles and signal analysis*. Oxford University Press, U.K. 507 pp

- Carper M, Porte-Agel F (2008) Subfilter-scale fluxes over a surface roughness transition. Part I: measured fluxes and energy transfer rates. *Boundary-Layer Meteorol* 126:157–179
- Castro IP, Cheng H, Reynolds R (2006) Turbulence over urban-type roughness: deductions from wind-tunnel measurements. *Boundary-Layer Meteorol* 118:109–131
- Cheng H, Castro IP (2002) Near-wall flow development after a step change in surface roughness. *Boundary-Layer Meteorol* 105:411–432
- Chew YT, Khoo BC, Li GL (1998) An investigation of wall effects on hotwire measurements using a bent sublayer probe. *Meas Sci Tech* 9:67–85
- Claussen M (1990) Area-averaging of surface fluxes in a neutrally stratified, horizontally inhomogeneous atmospheric boundary layer. *Atmos Environ* 24A(6):1349–1360
- Elliott WP (1958) The growth of the atmospheric internal boundary layer. *Trans Am Geophys Union* 39:1048–1054
- Garratt JR (1990) The internal boundary layer - a review. *Boundary-Layer Meteorol* 50:171–203
- Jensen NO (1978) Change of surface roughness and the planetary boundary layer. *Q J Roy Meteorol Soc* 104:351–356
- Jimenez J (2004) Turbulent flows over rough walls. *Annu Rev Fluid Mech* 36:173–196
- Khoo BC, Chew YT, Lim CP, Teo CJ (1998) Dynamic response of a hotwire anemometer. Part I: a marginally elevated hotwire probe for near-wall velocity measurements. *Meas Sci Technol* 9:751–763
- Mason PJ (1988) The formation of areally-averaged roughness lengths. *Q J Roy Meteorol Soc* 114:399–420
- Mulhearn PJ (1978) A wind-tunnel boundary layer study of the effects of a surface roughness change: rough-to-smooth. *Boundary-Layer Meteorol* 15:3–30
- Nemoto S (1972) Some considerations on the atmospheric internal boundary layer over the ground surface. *Meteorol Geophys* 23:121–134
- Panofsky HA, Townsend AA (1964) Change of terrain roughness and the wind profile. *Q J Roy Meteorol Soc* 90:147–155
- Patel VC (1965) Calibration of the preston tube and limitations on its use in pressure gradients. *J Fluid Mech* 23:185–208
- Rao KS, Wyngaard JC, Cote OR (1973) The structure of the two-dimensional internal boundary layer over a sudden change of surface roughness. *J Atmos Sci* 31:738–746
- Savelyev S, Taylor P (2005) Internal boundary layers: I. height formulae for neutral and diabatic flows. *Boundary-Layer Meteorol* 115:1–25
- Taylor PA (1987) Comments and further analysis on effective roughness lengths for use in numerical three-dimensional models. *Boundary-Layer Meteorol* 39:403–418
- Townsend AA (1965) The response of a turbulent boundary layer to abrupt changes in surface conditions. *J Fluid Mech* 22:799–822
- Townsend AA (1966) The flow in a turbulent boundary layer after a change in surface roughness. *J Fluid Mech* 26:255–266
- Wieringa J (1986) Roughness-dependent geographical interpolation of surface wind speed Averages. *Q J Roy Meteorol Soc* 112:867–889
- Wood DH (1982) Internal boundary layer growth following a step change in surface roughness. *Boundary-Layer Meteorol* 22:241–244